PAPER

PAPR reduction and performance enhancement of optical OFDM communication systems via migrating birds optimization-based SLM technique

To cite this article: Mahmoud Alhalabi *et al* 2026 *Eng. Res. Express* **8** 045318

Engineering Research Express

RECEIVED
3 December 2025

REVISED
7 February 2026

ACCEPTED FOR PUBLICATION
16 February 2026

PUBLISHED
26 February 2026

PAPER

PAPR reduction and performance enhancement of optical OFDM communication systems via migrating birds optimization-based SLM technique

Mahmoud Alhalabi[1,*], **Necmi Taşpınar**[2] and **Mohammed Wadi**[3]

[1] Department of Electrical and Electronic Engineering, Istanbul Yeni Yuzyil University, Istanbul, Türkiye
[2] Department of Electrical and Electronics Engineering, Erciyes University, Kayseri, Türkiye
[3] Department of Electrical and Electronic Engineering, Istanbul Sabahattin Zaim University, Istanbul, Türkiye
[*] Author to whom any correspondence should be addressed.

E-mail: mahmoud.alhalabi@yeniyuzyil.edu.tr, taspinar@erciyes.edu.tr and mohammed.wadi@izu.edu.tr

Keywords: PAPR, SLM, GA, MBO, PTS, DEHO, DIWO

Abstract

In Intensity-Modulated Direct Detection Optical Orthogonal Frequency Division Multiplexing (IM/DD-OOFDM) communication systems, a lower Peak-to-Average Power Ratio (PAPR) is essential for improving system performance. In order to reduce the high PAPR, a Migrating Birds Optimization (MBO) is integrated with the classical Selective Mapping (SLM) method in IM/DD-OFDM system. This approach successfully optimizes the values of phase factors, minimizes the search numbers, and reduces computational complexity. To evaluate the impact of the MBO-SLM method on PAPR reduction performance, the parameters of the MBO-SLM method play a crucial role in decreasing the PAPR in an IM/DD optical OFDM system. The MBO-SLM method demonstrates improved Bit Error Rate (BER) performance, Power Spectral Density (PSD), and power saving performance compared to other PAPR reduction methods. Numerical results indicate that the proposed PAPR reduction method outperforms other existing methods for optical OFDM signals. Specifically, by implementing this technique in the IM/DD optical OFDM communication system, we achieved a decrease in PAPR from 10.5 dB to 4.95 dB at a Complementary Cumulative Distribution Function (CCDF) of 10^{-3}, resulting in a reduction of 5.55 dB. Additionally, the computational complexity of the MBO-SLM method shows a 91% improvement over the Discrete Elephant Herding Optimization (DEHO) based Partial Transmit Sequence (PTS) method when the search number is set to 512.

1. Introduction

Optical communication systems are developing and improving with time to support high data rate transmission and provide more capacity. Nowadays, wired and wireless communication systems are still suffering from very low security, signal distortion and scattering, and limited bandwidth. Optical communications systems are the best choice for providing these advantages instead of wired and wireless communications. Additionally, Orthogonal Frequency Division Modulation (OFDM) technology is a popular and attractive method that supports high bit rate communication by reducing the effects of interference and noise [1]. The OFDM function first divides a high-input information stream into various low-data-rate sequences and then transmits signals by orthogonally placing the subcarriers. OFDM is a method used in optical communication systems to minimize the impact of inter-symbol interference (ISI) while maintaining high data communication speeds and bandwidth. However, the OFDM optical systems have a high peak to average power ration (PAPR). Due to its high PAPR, the Light Emitting Diode (LED) transmitter clips the transmitted optical signal, resulting in considerable distortion. Various solutions have been suggested to minimize PAPR, including partial transmit sequence (PTS), clipping and filtering, selective mapping (SLM), pre-coding, and post-coding [2]. The clipping technique induces in-band distortion by lowering the signal's amplitude to a specific level. Side

information transmission reduces bandwidth efficiency in the SLM method, while both post-coding and pre-coding techniques lower PAPR without affecting bit error performance (BER) performance [3]. Visible Light Communication (VLC) technology uses visible LEDs for real-time information transmission at very high speeds. According to [4], it can provide solutions for a widespread of applications, such as indoor navigation and localization (in situations where current GPS is unavailable), underground and underwater networks, and more. Extensive research has been conducted on Optical OFDM modulation for VLC systems to facilitate high-speed transmission [5]. OFDM provides resilience to frequency selective fading channels, enhances power efficiency, boasts high spectral efficiency, and tolerates multipath delay spread. A VLC network relies on intensity modulated and direct detected (IM/DD), requiring both positive and real-valued transmitted signals. VLC networks utilize various types of O-OFDM, such as DC-biased O-OFDM (DCO-OFDM), asymmetrically clipped Optical-OFDM (ACO-OFDM), Flip-OFDM, and asymmetrically clipped DC-biased optical-OFDM (ADO-OFDM). A DCO-OFDM network applies a DC bias to the optical OFDM signal to generate a unipolar signal. In ACO-OFDM, data symbols are transmitted solely on odd subcarriers, while even subcarriers are set to zero. In the Flip-OFDM transmission method, the negative and positive halves of the bipolar OFDM signal are sent over two separate frames. ADO-OFDM combines the features of both DCO-OFDM and ACO-OFDM. Briefly, the subcarriers are categorized as even and odd. ACO-OFDM uses odd sub-carriers, whereas DCO-OFDM uses even sub-carriers [6]. The transmitted signal must be clipped to zero to create a real and positive signal in ACO-OFDM [7]. However, designing OFDM systems still presents challenges. One of the most significant difficulties is the high PAPR of optical OFDM signals. The PAPR, determined by the total of orthogonal subcarriers generated by the inverse fast fourier transformation (IFFT) process at the transmitter, is the maximum to average power ratio. The non-linear characteristics of the LED in the transmitter cause the OFDM signal to shift, requiring a reduction in PAPR to prevent signal cutting and poor BER performance. Numerous PAPR reduction strategies have been described for optical OFDM signals [8]. In [9], the authors presented a PAPR reduction strategy for clipping that suffers from BER. In [10], the authors reduced the PAPR of the transmitted OFDM signal by recurrent clipping and filtering methods. Some PAPR reducing methods have been investigated like amplitude clipping and filtering, PTS, and SLM by Md. Milon *et al* in [11]. The authors in [12] studied PTS, SLM, tone reservation (TR), and PI as PAPR reduction methods. The authors in [13] compared PAPR reduction strategies in filter bank multicarrier (FBMC) and OFDM systems. In [14], the researchers introduced a machine learning (ML) strategy to reduce PAPR. Sanjana *et al* [15] developed a Hanowa matrix-based approach that improved the performance of the C-SLM method for reducing PAPR. Researchers in [16] have suggested an enhanced PTS PAPR reduction method that decreases BER, and power spectral density based on moth flame optimization. The authors in [17] have offered a method for reducing PTS PAPR based on m-vector. In [18], a two-stage (TR) method for reducing PAPR was proposed. In 2022, fuzzy neural networks were used to propose an adaptive PTS strategy to decrease PAPR in an OFDM system [19]. The iterative clipping and filtering (ICF) method [20] was simulated using three ways to minimize PAPR in an OFDM communication system. Authors in [21] proposed a hybrid Maximal-Minimum method with de-composed SLM to decrease PAPR limitations for 5G UFMC networks. Authors, in [22], proposed a new hybrid method, Low Complexity Hybrid SLM (LCHSLM), which combines modified SLM and companding to mitigate PAPR in ACO-OFDM systems. Researchers, in [23], reduce the computational complexity of the MIMO-OFDM system by integrating mapping signal sequences into the OFDM signals, which also improves PAPR reducing performance. A V Mayakannan *et al* [24] propose a neural network and linear regression method for PAPR reduction, achieving 84.1% reduction for 16QAM and 82.9% minimization for 64QAM-OFDM, without compromising BER. An improved PAPR reduction method has been suggested in 2021 using a quantum genetic algorithm (GA) and PTS, resulting in a 64% reduction in computational complexity [25]. Feng Zou *et al* reported a technique using neural networks for PAPR reduction, which is based on simplified clipping and filtering (SCF) techniques [26]. In [27], a method was presented for reducing the PAPR using a combination of mixed companding and clipping techniques. The SLM technique is a popular PAPR reduction algorithm due to its user-friendly structure and efficient performance without signal distortion. In the SLM method, a set number of phase sequences is generated at random. These sequences are then multiplied by the original data, which is modulated over quadrature amplitude modulation (QAM). The best phase sequence is selected based on the transmission signal with the lowest PAPR [28, 29]. The SLM algorithm requires one IFFT procedure for each randomly generated phase sequence, with the amount of searches increasing as the number of randomly produced phase sequences increases. As a result, SLM's computational complexity approaches extremely high values. Minimum search numbers must be used to find reasonable solutions in order to avoid this undesirable scenario. Furthermore, researchers have explored various methodologies to enhance the BER performance of optical OFDM communication systems. Specifically, recent studies [30–35] have introduced diverse optimization techniques aimed at mitigating signal degradation and improving overall transmission reliability.

In order to achieve this, we applied an advanced new method for the optical OFDM system known as migrating birds optimization (MBO) with SLM (MBO–SLM). This technique uses MBO-based phase factors optimization iteratively to achieve better solutions with fewer search values [36]. While various metaheuristic algorithms such as GA, Particle Swarm Optimization (PSO), and Differential Evolution (DE) have been applied to SLM, MBO offers distinct theoretical advantages specifically suited to the discrete phase sequence optimization problem. Unlike GA, which relies on crossover operators that can disrupt high-quality partial solutions (building blocks) in discrete spaces, or PSO, which requires complex discretization processes for phase selection, MBO utilizes a unique 'benefit mechanism' through its V-formation structure. In this structure, the leader solutions share unvisited, high-quality neighbor solutions with follower solutions. This mechanism inherently prevents the loss of promising search directions—a common issue in standard population-based heuristics—and balances global exploration with local exploitation more effectively. Consequently, MBO is hypothesized to converge to optimal phase factors with fewer function evaluations than its evolutionary counterparts, addressing the critical constraint of computational complexity in optical OFDM systems.

Recent advancements have also introduced Deep Learning (DL) techniques for PAPR reduction, offering adaptive optimization with potentially lower complexity for 5G systems [37]. These data-driven approaches represent a significant parallel development to the metaheuristic methods explored in this work.

The primary contributions of this work are:

1. An enhanced MBO-SLM approach was utilized and applied to our proposed optical OFDM system to reduce PAPR.
2. The MBO algorithm has been utilized to reduce PAPR in optical IM/DD OFDM systems.
3. We investigated various techniques for reducing PAPR, including discrete elephant herding optimization-based PTS (DEHO-PTS), discrete crow search algorithm-based PTS (DCSA-PTS), discrete invasive weed optimization-based PTS (DIWO-PTS), SLM, and GA-SLM. We provided a detailed comparison of their performance in terms of PAPR reduction, BER performance, power spectral density (PSD) performance, power saving performance, and computational complexity.

The organization of the remainder of the paper is as follows: section 2 outlines the fundamental operating principles of the O-OFDM system and discusses the principle of PAPR in our proposed optical OFDM system. Section 3 explains the PAPR reduction method including the MBO-SLM method. Section 4 describes the MBO-SLM technique. Section 5 presents the simulation outcomes, and section 6 contains the conclusions.

2. System description

Optical OFDM (O-OFDM) types can be classified as coherent detection OFDM (CO-OFDM) or direct detection optical OFDM (DDO-OFDM), depending on the method of detection. DDO-OFDM can be classified into two types: Linearly mapped DDO-OFDM (LM-DDO-OFDM) and non-linearly mapped OFDM (NLM-DDO-OFDM). NLM-DDO-OFDM systems are intensity-modulation optical OFDM communication systems, where the intensity of the transmitted optical signal represents the electrical signal. Examples of this method include optical wireless systems, plastic optical fiber systems, and multimode optical fibers. The IM/DD approach ensures intensity modulation without information loss by requiring a true and positive input signal. The IFFT block's input is subject to limitations such as Hermitian symmetry. Figure 1 shows the block diagram of an IM/DD optical OFDM system. The IFFT/FFT block plays a critical role in processing signals for both the transmitter and the receiver, serving as the central component of the system. The FT technique converts time-domain input data into a frequency-domain data signal. Various types of FT are utilized depending on the network's application. Traditional FT transmits continuous signals in the time/frequency domain, simplifying signal processing by sampling them in the traditional transformation.

Fast algorithms FFT and IFFT are widely used in digital signal processing applications to get the DFT and IDFT. Optical OFDM systems utilize IFFT for modulation at a transmitter and FFT for demodulation at a receiver. The IFFT is a method that uses a complex input vector as $S = (S_0, \ldots, S_{N\text{-}1})$, where S represents the modulated input information sequence, and N represents the total amount of subcarriers [38].

Since IM/DD optical systems require the transmitted signal to be real-valued, the frequency-domain input to the IFFT must satisfy Hermitian symmetry. To achieve this while accommodating N independent information subcarriers, we utilize a $2N$-point IFFT. The input vector S_H of length $2N$ is constructed as follows:

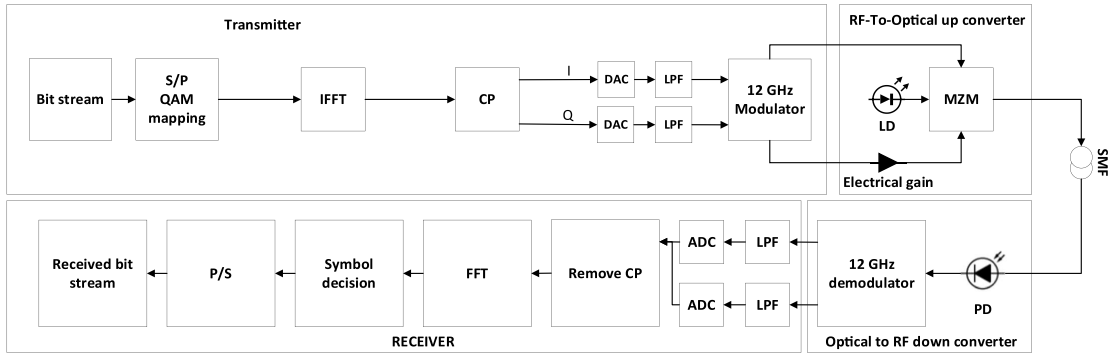

Figure 1. Block diagram of an IM/DD optical OFDM system. S/P: Serial to parallel. IFFT: Inverse Fast Fourier Transformation. CP: Cyclic Prefix. DAC: Digital to Analog Converter. LPF: Low Pass Filter. MZM: Mach–Zehnder Modulator. SMF: Single Mode Fiber. PD: Photodetector. P/S: Parallel to Serial.

$$\boldsymbol{S_H(k)} = \begin{cases} S(k)\ 1 \leqslant k < N \\ 0\ k = 0,\ N \\ \boldsymbol{S}^*(2N - k) N < k < 2N \end{cases} \tag{1}$$

where $S(k)$ represents the QAM-modulated data symbols, and $(\cdot)^*$ denotes the complex conjugate. The components at DC ($k = 0$) and the Nyquist frequency ($k = N$) are set to zero to strictly maintain symmetry and signal integrity. Consequently, the real-valued time-domain OFDM signal $s(n)$ is obtained via the $2N$-point IFFT:

$$\boldsymbol{s(n)} = \frac{1}{2N} \sum_{k=0}^{2N-1} \boldsymbol{S_H(k)} e^{j\frac{2\pi nk}{2N}}, \quad 0 \leqslant \boldsymbol{n} < 2\boldsymbol{N} \tag{2}$$

The PAPR of any OFDM signal is the ratio of its peak power to its average power in the time domain as follows:

$$\boldsymbol{PAPR(dB)} = 10\log_{10} \frac{\max\ |\boldsymbol{s(n)}|^2}{\boldsymbol{E}\ \{\boldsymbol{s(n)}^2\}}. \tag{3}$$

In this context, max $|\boldsymbol{s(n)}|^2$ represents the highest power value of the OFDM signal, while E[.] represents the average of those values. The CCDF of *PAPR* is a common statistic that shows a reduction in *PAPR*. It measures how likely it is that the PAPR of an OFDM frame will exceed a certain threshold called $PAPR_0$ [39, 40].

$$CCDF = Prob(PAPR > PAPR_0). \tag{4}$$

2.1. Physical relationship between PAPR, nonlinearity, and BER

To fully understand the BER improvements reported in this work, it is necessary to model the quantitative relationship between PAPR and the optical transmitter's nonlinearity. The optical transmitter (whether an LED or MZM) is inherently limited by a dynamic range defined by a minimum power $P_{\min}$ and a maximum saturation power $P_{\max}$.

When the high-PAPR OFDM signal $s(n)$ exceeds these thresholds, it undergoes clipping. This non-linear distortion can be modeled as an additional noise source. The distorted transmitted signal $s_{out}(n)$ is given by:

$$\boldsymbol{s_{out}(n)} = \boldsymbol{s(n)} + \boldsymbol{s_{clip}(n)} \tag{5}$$

where $s_{clip}(n)$ represents the clipping noise. According to the Bussgang theorem, this clipping noise is uncorrelated with the input signal and acts as additive interference. The power of this clipping noise, σ^2_{clip}, is directly related to the probability of the signal peaks exceeding the transmitter's linear limit (the clipping threshold).

The BER at the receiver is a function of the effective Signal-to-Interference-plus-Noise Ratio (SINR), which is degraded by this clipping noise:

$$SINR = \frac{P_{avg}}{\sigma^2_{thermal} + \sigma^2_{clip}} \tag{6}$$

where P_{avg} is the average signal power and $\sigma^2_{thermal}$ is the receiver's thermal noise variance.

By reducing the PAPR, the MBO-SLM method effectively compresses the signal's probability density function into the linear region of the transmitter [$P_{\min}$, $P_{\max}$]. This minimizes the occurrence of clipping events,

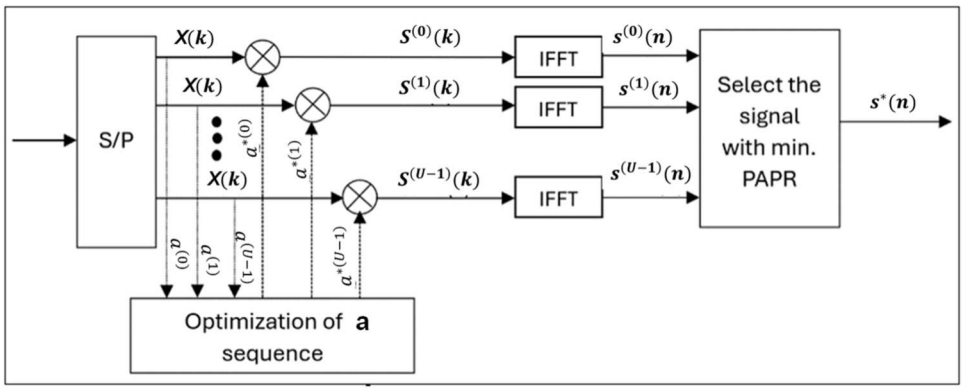

Figure 2. An OFDM transmitter's schematic design using the MBO-SLM technique.

thereby significantly reducing the clipping noise variance σ^2_{clip}. As $\sigma^2_{clip} \rightarrow 0$, the SINR maximizes, leading directly to the improved BER performance observed in the simulation results.

3. PAPR reduction based on the MBO-SLM method in the optical OFDM transmitter

Figure 2 shows the schematic diagram of the optical OFDM transmitter after integrating the MBO-SLM method.

Firstly, the information bits are transformed into different symbols by using any QAM modulation, and the QAM symbols are represented below:

$$\boldsymbol{S(k)} = [\boldsymbol{S}(0), \ldots, \boldsymbol{S}(\boldsymbol{N}-1)]. \tag{7}$$

After that, the vector of $S(k)$ is multiplied by the optimized N length different phase rotation factor vectors $a^{*(u)}(k) = [a^{*(0)}(0), ., a^{*(u)}(N-1)]$ generated randomly, which $a^{*(u)}(k)$ *including* -1 *and* $1, u = 1,\ldots, U$. The variable U represents the number of phase factor combinations that are randomly generated.

The frequency-domain candidate vector $S^{(u)}$ for the u-th phase sequence is generated by the element-wise multiplication of the original data vector S and the phase vector $a^{(u)}$. This operation is compactly expressed using the Hadamard product notation ($\odot$) as:

$$S^{(u)} = S \odot a^{*(u)}. \tag{8}$$

In component-wise form, the k-th subcarrier of the u-th candidate sequence is defined as:

$$\boldsymbol{S^{(u)}(k)} = \boldsymbol{S(k)} \cdot \boldsymbol{a^{*(u)}(k)}, \quad \boldsymbol{k} = 0, 1,\ldots,\boldsymbol{N}-1. \tag{9}$$

Following the multiplication step, the optimized phase-rotated data sequence symbolized by $S^{(u)}(k)$ is expressed as below:

$$\boldsymbol{S^{(u)}(k)} = [\boldsymbol{S}(0) \times \boldsymbol{a^{*(u)}}(0),\ldots., \boldsymbol{S}(\boldsymbol{N}-1) \times \boldsymbol{a^{*(u)}}(\boldsymbol{N}-1)] = [\boldsymbol{S^{(u)}}(0), ,\ldots .., \boldsymbol{S^{(u)}}(\boldsymbol{N}-1)] \tag{10}$$

The IFFT operation is applied to the optimized phase-rotated data vector to obtain the following time domain signal:

$$\begin{aligned} \boldsymbol{s^{(u)}(n)} &= [\boldsymbol{s^{(u)}}(0),\ldots., \boldsymbol{s^{(u)}}(\boldsymbol{N}-1)] \\ &= \boldsymbol{IFFT}(\boldsymbol{S^{(u)}(k)}) \\ &= \frac{1}{\sqrt{\boldsymbol{N}}} \sum_{\boldsymbol{k}=0}^{\boldsymbol{N}-1} \boldsymbol{S(k).a^{*(u)}(k).e^{j\frac{2\pi k}{N}n}}, \ 0 \leqslant \boldsymbol{n} \leqslant \boldsymbol{N}-1, \ \boldsymbol{u} = 1,\ldots, \boldsymbol{U}. \end{aligned} \tag{11}$$

After generating the time-domain candidates, the PAPR is calculated for each of the U alternative OFDM sequences. The transmitter then selects the specific candidate sequence $s^{(\tilde{u})}(n)$ that results in the lowest PAPR. The selection of the optimal phase factor index $\tilde{u}$ is defined as:

$$\tilde{\boldsymbol{u}} = \arg \min_{1 \leqslant \boldsymbol{u} \leqslant \boldsymbol{U}} \{\boldsymbol{PAPR}\{\boldsymbol{s^{(u)}(n)}\}\}. \tag{12}$$

Consequently, the transmitted signal $s^*(n)$ corresponds to the candidate sequence associated with this optimal index:

$$\boldsymbol{s^*(n)} = \boldsymbol{s^{(\tilde{u})}(n)}. \tag{13}$$

where PAPR$\{\cdot\}$ represents the calculation defined in equation (3).'

4. MBO-SLM technique

Duman and his team developed the MBO algorithm, inspired by the *V*-designed construction of travelling birds, which maximizes distance with minimal energy [41]. According to [36], The phase sequences can be represented as bird positions in the subsequent form:

$$\boldsymbol{a}^{(f)}(\boldsymbol{k}) = [\boldsymbol{a}^{(f)}(0),\ldots,\boldsymbol{a}^{(f)}(\boldsymbol{N}-1)],\ f = 1,\ ..,\ F. \tag{14}$$

F represents the total amount of birds in the swarm. The neighboring solutions for the associated element locations are represented as follows:

$$\boldsymbol{p}^{(f,w)}(\boldsymbol{k}) = [\boldsymbol{p}^{(f,w)}(0),\ldots,\boldsymbol{p}^{(f,w)}(\boldsymbol{N}-1)],\ \mathrm{w} = 1,\ldots,\ \mathrm{W} \tag{15}$$

$\boldsymbol{p}^{(f,w)}(\boldsymbol{k})$ denotes the *w*th neighboring solution of the *f*th element. *W* is the total amount of neighboring elements for every bird. The optimization of phase factor sequences are carried out using MBO-SLM as follows:

Step 1: An additional dimension is inserted into both the element and neighboring locations to maintain fitness values as indicators of solution quality. The updated definitions for bird and neighbor solution vectors are:

$$\boldsymbol{Y}^{(f)}(\boldsymbol{k}) = [\boldsymbol{a}^{(f)}(0),\ldots,\boldsymbol{a}^{(f)}(\boldsymbol{N}-1),\ \boldsymbol{fit}(\boldsymbol{a}^{(f)}(\boldsymbol{k}))]. \tag{15}$$

$$\boldsymbol{Z}^{(f,w)}(\boldsymbol{k}) = [\boldsymbol{p}^{(f,w)}(0),\ldots,\boldsymbol{p}^{(f,w)}(\boldsymbol{N}-1),\ \boldsymbol{fit}(\boldsymbol{p}^{(f,w)}(\boldsymbol{k}))]. \tag{16}$$

$fit(\boldsymbol{a}^{(f)}(\boldsymbol{k}))$ and $fit(\boldsymbol{p}^{(f,w)}(\boldsymbol{k}))$ indicate the fitness rates of $\boldsymbol{a}^{(f)}(\boldsymbol{k})$ and $\boldsymbol{p}^{(f,w)}(\boldsymbol{k})$, respectively. To initialize the solution vectors $\boldsymbol{Y}^{(f)}(\boldsymbol{k})$, random phase sequences are generated, and fitness values are calculated as follows:

$$\boldsymbol{fit}(\boldsymbol{a}^{(f)}(\boldsymbol{k})) = \max_{0\leqslant \boldsymbol{n}\leqslant \boldsymbol{N}-1}\left[\left|\frac{1}{\sqrt{\boldsymbol{N}}}\sum_{\boldsymbol{k}=0}^{\boldsymbol{N}-1}\boldsymbol{S}(\boldsymbol{k}).\,a^{(f)}(k).\boldsymbol{e}^{\frac{\boldsymbol{j2\pi kn}}{\boldsymbol{N}}}\right|^2\right],\ f = 1,\ ..,\ F. \tag{17}$$

$\boldsymbol{Y}^{(f)}(\boldsymbol{k})$ vectors, each representing an individual bird, are organized in a V shape.

It is important to note that the phase factors $\boldsymbol{a}^{(f)}(\boldsymbol{k})$ are selected from the set $\{-1,\ 1\}$, which inherently have unit magnitude. Consequently, the element-wise multiplication in the frequency domain does not alter the magnitude of the subcarriers. According to Parseval's theorem, the total energy—and thus the average power $E[|s_n|^2]$—of the time-domain signal remains constant across all candidate phase sequences. Since the denominator in the PAPR equation (equation (6)) is constant for all candidates, minimizing the maximum instantaneous power (the numerator) in equation (17) is mathematically equivalent to minimizing the PAPR.

Step 2: The *W* neighboring birds of the leader bird are formed after the initialization process. The cyclic bit-flipping process is integrated into the MBO algorithm to optimize the generation of neighbors, enhancing a phase sequence of positive and negative values [36]. An additional dimension in the solution vectors allows for the cyclic bit-flipping process.

$$\boldsymbol{Y}^{(f)}(\boldsymbol{k}) = [\boldsymbol{a}^{(f)}(\boldsymbol{k}),\ \boldsymbol{fit}^{(f)}(\boldsymbol{k}),\ \boldsymbol{m}_f)]. \tag{18}$$

$$\boldsymbol{Z}^{(f,w)}(\boldsymbol{k}) = [\boldsymbol{p}^{(f,w)}(\boldsymbol{k}),\ \boldsymbol{fit}(\boldsymbol{p}^{(f,w)}(\boldsymbol{k})),\ \ \boldsymbol{m}_{f,w})]. \tag{19}$$

where $\boldsymbol{m}_f$ and $\boldsymbol{m}_{f,w}$ denote the index values associated with the *f*-th solution and the *f*-th solution's *w*-th neighbor, respectively. The neighbor generation method, which is based on cyclic bit flipping, will make use of these solution-specific index values. The initial index value for all birds is set to $\mathrm{m}_f = 1$. Later, the leader bird's first neighbor solution is created using the next equation (for $w = 1, f = 1$):

$$\boldsymbol{Z}^{(f,w)}(\boldsymbol{k}) = \boldsymbol{flip}\ (\boldsymbol{Y}^{(f)}(\boldsymbol{k}))_{\boldsymbol{m}_f}. \tag{20}$$

The function $flip(\boldsymbol{Y}^{(f)}(\boldsymbol{k}))$ changes the mark of the m_f-th phase factor in the vector $\boldsymbol{Y}^{(f)}(\boldsymbol{k})$, which takes values from $\{-1, 1\}$. The flipping index, denoted as m_f, increases by 1 after the bit-flipping operation:

$$\boldsymbol{m}_f = \ \boldsymbol{m}_f + 1. \tag{21}$$

The subsequent bit-flipping process for every neighbor production starts from the phase weighting sequence next to the one that was previously flipped. After increasing m_f by 1, the flipping operation is performed cyclically in the next equation:

$$\boldsymbol{m}_f = \ \boldsymbol{mod}\ (\boldsymbol{m}_f - 1,\ \boldsymbol{N}) + 1. \tag{22}$$

The expression $mod(m_f - 1, N)$ uses the modulo process on m_f - 1 to N. As a result, the mf value of the *f*th solution vector, represented by $\boldsymbol{Y}^{(f)}(\boldsymbol{k})$, is raised by 1 for each neighbor generation. Equation (22) returns to the starting value of 1 after a few algorithm cycles, when the value of m_f approaches $N + 1$. This cycle keeps going until the optimization process is finished for every solution vector. The cyclic bit-flipping process reduces the number of unvisited neighbor solutions for the population elements. The value of $m_{f,w}$ equals the value of m_f after m_f has been updated using equation (22):

Table 1. Key symbols and parameters.

Symbol	Definition
N	Number of subcarriers (IFFT/FFT size)
U	Number of candidate phase sequences in the SLM block
F	Number of birds in the flock (Population size)
W	Number of neighbor solutions generated for each bird
H	Number of neighbor solutions shared with follower birds
T	Number of tours per cycle
C	Number of cycles (flock reorganizations)
m_f	Cyclic bit-flipping index for the f-th bird
X_H	Hermitian-symmetric frequency-domain vector
$x^*(n)$	Transmitted time-domain signal with minimum PAPR

$$\boldsymbol{m_{f,w}} = \boldsymbol{m_f}. \tag{23}$$

The neighbor $\boldsymbol{Z}^{(f,w)}(\boldsymbol{k})$ replaces $\boldsymbol{Y}^{(f)}(\boldsymbol{k})$, producing the wth neighbor of the fth solution vector through a bit-flipping process from the member next to the m_fth phase weighting factor sequence. The first neighboring of the leader solution is generated by equation (20)–(23) and repeated till W neighbors are obtained. The leader solution vectors are arranged based on their fitness qualities, which are evaluated as below:

$$\boldsymbol{fit}\left(\boldsymbol{p}^{(f,w)}(\boldsymbol{k})\right) = \max_{0\leqslant \boldsymbol{n}\leqslant \boldsymbol{N}-1}\left[\left|\frac{1}{\sqrt{\boldsymbol{N}}}\sum_{\boldsymbol{N}-1}^{\boldsymbol{k}=0}\boldsymbol{S}(\boldsymbol{k}).\,p^{(f,w)}(k).\boldsymbol{e}^{\frac{\boldsymbol{j2\pi kn}}{\boldsymbol{N}}}\right|^2\right]$$
$$w = 1,\ldots,W. \tag{24}$$

The SLM technique optimizes phase factors through a reduction problem, selecting the neighbor solution with the lowest fitness value as the top choice. If the best neighboring solution has higher fitness than the leader solution, it replaces the leader. The top two unused neighboring solutions ($2H$) are then shared with the second and third elements behind the leader using the second-best neighbor solution. Each follower receives a certain amount of solutions, denoted by H. The second bird receives even-indexed solutions, whereas the third bird receives odd-indexed ones.

Step 3: The (W - H) neighbor solutions are generated for each remaining bird, except the leader, using equations (20)–(23). The fitness function specified in equation (24) is used to evaluate the neighbor solutions. To reach a total of W neighbors, the greatest unused H neighbor solutions from the front element are inserted into the group. The final neighbor group is created by merging the H neighbor solutions that the element in front and its ($W-H$) produced neighbor solution shared. The solutions in this group are then graded based on their fitness ratings. The associated bird is updated by the neighboring solution if the best fitness in the neighboring group surpasses that of the element. The follower bird is then given access to the best underused H neighbor solutions. A tour is completed after all remaining solutions, except the first, have been executed in Step 2.

Step 4: After completing the specified total amount of tours (T), the leader element shifts to the left end tail of the swarm in a V shape, while the second element on the left takes over the leader location. To change leaders, the leader one moves to the right end tail of the swarm and the third element on the right direction takes the leader's location. One cycle of the algorithm is finished by performing the leader replacement operation. After executing steps 2–4 for a certain amount of cycles (C), the algorithm terminates, and the element with the greatest fitness rate is selected. The MBO algorithm optimizes the phase sequence, resulting in the optimum signal $s^*(n)$ from the MBO-SLM block output. Table 1 summarizes the key symbols and parameters used throughout the paper.

5. Simulation results

The Optisystem software was used to simulate the optical system architecture and visualize the results of simulation and MATLAB software tool is used to build the script of OFDM transmitter and receiver, and show the PAPR reduction performance evaluations. As shown in figure 1, our proposed IM/DD optical OFDM communication network consists of three parts: RTO transmitter at the central office, fiber optic channel, and OTR receiver. The BER test set component provides a total system bit rate of 40 Gb s^{-1} and is utilized at the central office to produce digital bits. Additionally, it is used to compare the bit rates of transmitted and received

Table 2. The primary parameters of the simulation.

Type	Parameter name	Value
System parameters	Sequence Length	262144
	Samples per Bit	4
	Bit Rate	40 Gbps
	Number of samples	2097152
	Symbol Rate	$10e^9$ Symbols/s (16-QAM)
OFDM modulator	FFT points	128
	Number of used subcarriers	80
	Cyclic prefix	5
CW laser	Operating frequency	193.1 THz (1552 nm)
	Output Power	1.2 mW
	Line width	0.01 MHz
PIN photodetector	Dark current	10 nA
	Responsivity type	InGaAs

data. A total of 128 FFT points are used, along with 80 subcarriers. Table 2 lists all the parameters of system OFDM modulator, CW laser, and the photodetector.

The QAM sequence generator converts generated bits into QAM symbols, which are modulated into several orthogonal subcarriers in an OFDM modulator. However, the subcarriers and FFT point numbers are set to 80 and 128, respectively. The I-Q OFDM signals will be processed through a low pass filter with a cutoff frequency of 12.4 GHz. Quadrature modulators increase the frequency of transmitted OFDM signals to 12 GHz. The transmitted RF electrical signal is transformed to the optical field utilizing Mach–Zehnder modulator (MZM). The CW laser and PIN photo-detector parameters are listed in table 2, respectively.

Following MZM, the optical signal is sent over (20+10×no. loops) of single-mode fiber (SMF). DCF reduces the dispersion caused by the primary optical fiber and enhances communication performance. The transmitted signal is amplified by another amplifier within the loop, compensating for any loss. The amplified optical signal is filtered using a filter with a central frequency of 193.1 THz and a bandwidth of 50 GHz. In the receiver, the optical signal is transformed into an electrical signal by the PIN photodetector. The electrical signal that is received is amplified by an electrical amplifier. The amplified received signal is demodulated and recovered by a quadrature demodulator. The OFDM modulator and demodulator must have identical parameters to recover transmitted QAM symbols accurately. Finally, the QAM sequence detector converts the received symbols to bits per symbol. The BER test set is utilized to assess BER and its log accurately.

Figure 3 illustrates the CCDF of PAPR for the various reduction techniques. It is evident that while all metaheuristic-based methods improve upon the original OFDM signal (10.5 dB), the MBO-SLM approach achieves the most significant reduction, reaching 4.95 dB at a CCDF of 10^{-3}. This superior performance—surpassing GA-SLM by 0.44 dB and classical SLM by 0.55 dB under identical search constraints ($SN = 512$)—can be attributed to the MBO algorithm's unique 'neighbor sharing' mechanism. Unlike the independent random trials in classical SLM or the crossover operations in GA, the V-formation structure in MBO allows follower solutions to exploit promising phase trajectories discovered by leader solutions, thereby converging to deeper local minima in the phase optimization landscape. When DCSA-PTS was used, the PAPR value was slightly reduced compared to DEHO-PTS. For the PTS technique, DIWO-PTS significantly reduced the PAPR and gave the best PAPR reduction performance compared to DEHO-PTS and DCSA-PTS [42]. When GA-SLM was used, the PAPR value was 5.39 dB at CCDF = 10^{-3} when the population number was 32 and the generation number was 16, crossover rate was 0.6, and mutation rate was 0.01. When MBO-SLM was used, the PAPR value was 4.97 dB at CCDF = 10^{-3} when the amount of searches was 512. After GA-SLM was applied to the proposed IM/DD optical OFDM system, the PAPR was minimized from 10.5 dB to 5.39 dB at CCDF of 10^{-3}, this led to a decrease of 5.11 dB as in table 3. After MBO-SLM was applied to our proposed IM/DD optical OFDM communication system, the PAPR was decreased from 10.5 dB to 4.95 dB at CCDF of 10^{-3}, leading to a reduction of 5.55 dB as in table 3. From table 3, it is stated that MBO-SLM provides lower PAPR values than other methods. To ensure a fair computational comparison across all methods, the Search Number (SN) is strictly defined as the total number of IFFT operations required by the transmitter. In the conventional SLM scheme, SN corresponds directly to the number of parallel candidate phase sequences (U), as each requires one IFFT. Similarly, for the metaheuristic-assisted approaches (MBO, GA, DEHO, etc), determining the fitness of any candidate solution requires transforming the frequency-domain signal into the time domain to measure its peak power. Consequently, every iterative fitness evaluation necessitates exactly one IFFT operation. Since the computational complexity of the IFFT block ($O(N \log_2 N)$) overwhelmingly dominates the linear complexity of internal algorithmic operations (such as phase generation, crossover, or bit-flipping), equating the total number of

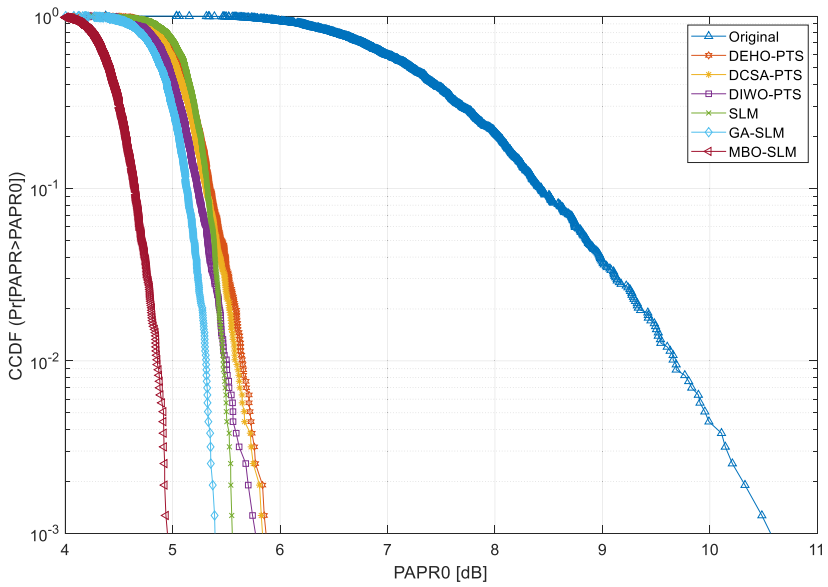

Figure 3. $PAPR_0$ [dB]—CCDF curves of all simulated methods.

Table 3. Search parameters (Search Number) and resulting PAPR values for all simulated methods.

Technique	Search number (SN)	PAPR (dB)
Original	0	10.5
DEHO based on PTS	$C \cdot E \cdot MIN = 2 \cdot 16 \cdot 16 = 512$	5.86
DCSA based on PTS	$S \cdot t. = 2 \cdot 256 = 512$	5.83
DIWO based on PTS	$NFE = 512$	5.77
SLM	$U = 512$	5.5
GA based on SLM	$P.G = 32.16 = 512$	5.39
MBO based on SLM	$[W + (W—H).(F—1)]\,.T.C = 512, F = 5; H = 1; W = 4; C = 8; T = 4$	4.95

fitness evaluations in MBO-SLM to the number of candidate sequences in classical SLM provides a rigorous and consistent metric for complexity analysis.

It is also crucial to distinguish the source of these performance gains. The superior reduction in PAPR achieved by MBO-SLM is attributable to the algorithm's intrinsic 'neighbor sharing' property rather than arbitrary parameter tuning. By allowing following 'birds' (candidate solutions) to inherit the best unused search trajectories of leading candidates, the algorithm effectively recycles computational effort that other algorithms (like GA or others) would discard. This structural efficiency allows MBO-SLM to locate lower-PAPR phase sequences within the same search limit ($N = 512$) where other heuristics stagnate, demonstrating that the improvement is algorithmic rather than merely parametric.

Figure 4 examines the impact of various high modulation orders on the performance of MBO-SLM method, analyzing the PAPR curves for 16, 32 and 64 QAM, respectively. Figure 4 shows that the high modulation orders have a minimal impact on the performance of PAPR reduction. At a CCDF of 10^{-3}, the difference in PAPR among different M-QAM orders is 0.05 dB as shown in figure 4.

The overall power spectral density (PSD) of the signal is calculated by summing the PSDs of all individual subcarriers. Because the subcarriers are orthogonal, their power contributions combine constructively, leading to a flat overall PSD across the frequency range they occupy. The flat PSD shows a uniform power distribution across the subcarriers, effectively utilizing the available spectrum. Figure 5 presents the PSD analysis, highlighting the impact of PAPR reduction on out-of-band radiation. High PAPR peaks in the time domain typically drive the optical transmitter into saturation, causing non-linear clipping distortion that manifests as spectral regrowth (side-lobes) in the frequency domain. As shown in the figure, the MBO-SLM method achieves the lowest out-of-band radiation level of approximately -74 dBm Hz^{-1}. This 11 dB improvement over the DEHO-PTS method (-63 dBm Hz^{-1}) confirms that the superior PAPR reduction of MBO-SLM effectively mitigates the non-linear clipping noise, thereby preserving the spectral compactness of the optical OFDM signal.

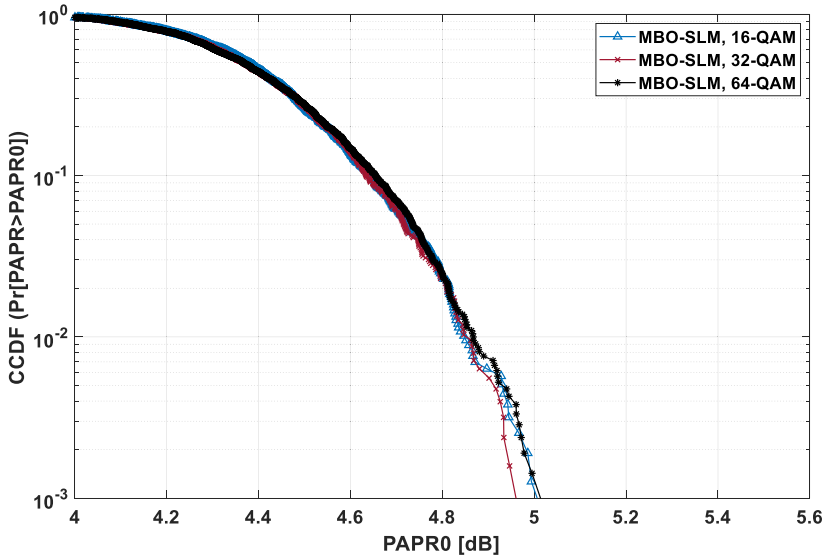

Figure 4. CCDF of PAPR for MBO-SLM applied to 16-, 32-, and 64-QAM.

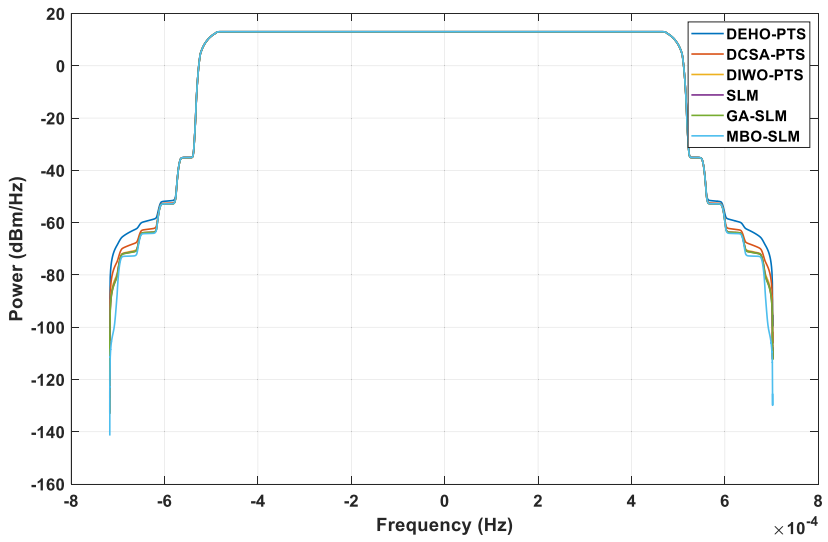

Figure 5. PSD analysis of optical OFDM spectrum after using PAPR reduction methods for the 16-QAM modulation.

In comparing methods for PAPR reduction, it is essential to consider power-saving performance. This performance is defined by:

$$\textit{Power saving}\ (\%) = \frac{\textit{Original PAPR value} - \textit{Reduced PAPR value}}{\textit{Original PAPR value}} \times 100 \tag{25}$$

Table 4 evaluates the power-saving performance of six PAPR reduction techniques for 16-QAM, with MBO-SLM achieving the highest efficiency at 52.9%, followed by GA-SLM (48.7%) and conventional SLM (47.6%), demonstrating that metaheuristic-enhanced SLM methods consistently outperform standalone PTS variants. Among PTS-based approaches, DIWO (45%) slightly surpasses DCSA (44.5%) and DEHO (44.2%), suggesting that bio-inspired optimizations (e.g., Invasive Weed Optimization) marginally improve power efficiency over DEHO or DCSA. The superior performance of MBO-SLM highlights the potential of nature-inspired algorithms in optimizing phase sequences for PAPR reduction, though computational complexity and BER trade-offs must be assessed to determine practical applicability.

Figure 6 depicts the BER performance as a function of the OSNR. The results demonstrate a clear correlation between PAPR reduction capability and BER improvement. The MBO-SLM method exhibits the best performance, requiring approximately 1.5 dB less OSNR than GA-SLM and 9 dB less than the original OFDM signal to achieve a BER of 10^{-4}. This gain is physically justified by the reduction in clipping noise; by

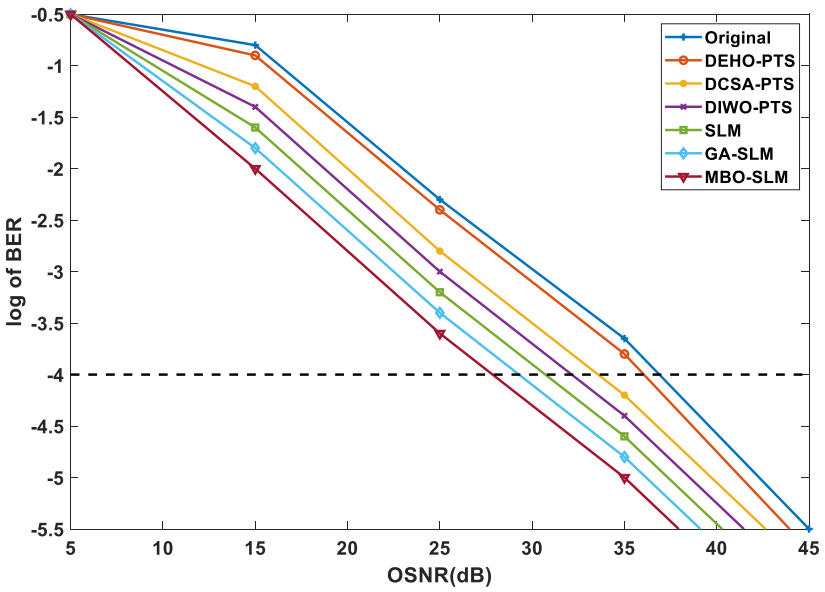

Figure 6. BER performance results for each of the PAPR reduction techniques considered.

Table 4. Power saving performance of PAPR reduction methods for 16-QAM.

PAPR reduction method	16-QAM (10.5 dB)
DEHO based on PTS	44.2%
DCSA based on PTS	44.5%
DIWO based on PTS	45%
SLM	47.6%
GA-SLM	48.7%
MBO-SLM	52.9%

compressing the signal's dynamic range, MBO-SLM ensures that the transmitted waveform remains largely within the linear region of the LED. This maximizes the effective Signal-to-Interference-plus-Noise Ratio (SINR) at the receiver, directly translating to the observed improvement in error rates. While the OSNR value will be fixed, the BER of the optical OFDM signal based on DEHO-PTS method is the maximum; but the BER of the DCSA-PTS method is less than that of the DEHO-PTS method. While the BER equals 10^{-4}, the MBO-SLM technique needs about 1.5 dB fewer OSNR compared to the GA-SLM technique, about 2.86 dB fewer OSNR compared to the conventional SLM technique, about 4.3 dB fewer OSNR compared to the DIWO-PTS technique, about 5.7 dB fewer OSNR compared to the DCSA-PTS technique, about 8.1 dB fewer OSNR compared to the DEHO-PTS technique, and about 9 dB fewer OSNR compared to the original OFDM signal. The MBO-SLM technique provides better BER performance than other techniques.

To observe the outcome of various $\{F,\ W,\ H,\ T,\ C\}$ groupings on the PAPR reduction performance of the MBO-SLM method, the $PAPR_0$ [dB]—CCDF curve is analyzed in figure 7 for different parameter combinations satisfying the search complexity equation $SN = [(F-1)\cdot(W+(W-H))]\cdot C\cdot T = 512$. The specific groupings investigated for this research include $\{3,\ 14,\ 5,\ 4,\ 4\}\$,\ \$\{5,\ 4,\ 1,\ 4,\ 8\}$, $\{5,\ 8,\ 2,\ 4,\ 4\}, \{7,\ 10,\ 1,\ 2,\ 4\}, \{9,\ 8,\ 1,\ 2,\ 4\}$, and $\{9,\ 16,\ 2,\ 2,\ 2\}$. To ensure these combinations maintain a search complexity equal to 512, two additional conditions were enforced: first, the F value must be an odd number to produce a symmetric V-shaped flock, and second, the total number of neighbor solutions W must satisfy $W \geqslant (2H+1)$ to ensure that each follower bird has sufficient unused neighboring solutions from the element ahead of it.

The results in figure 7 indicate that the best PAPR minimization performances are achieved with lower bird count combinations, specifically $\{5,\ 4,\ 1,\ 4,\ 8\}, \{5,\ 8,\ 2,\ 4,\ 4\}$, and $\{3,\ 14,\ 5,\ 4,\ 4\}$, whereas population sizes larger than 5 lead to significantly poorer performance. Notably, the optimal parameter grouping is identified as $\{5,\ 4,\ 1,\ 4,\ 8\}$ and $\{5,\ 8,\ 2,\ 4,\ 4\}$ which achieve a PAPR value of approximately 5 dB at $CCDF = 10^{-3}$.

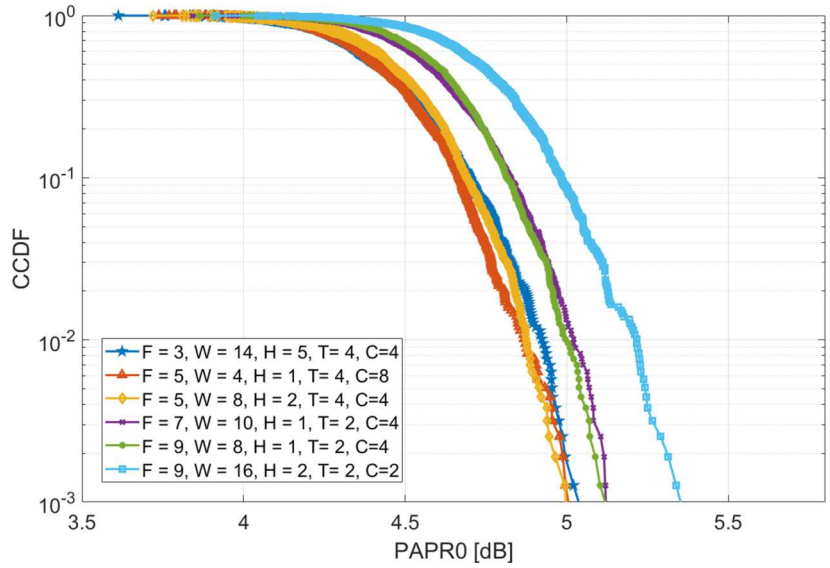

Figure 7. The impact of various parameter groupings on PAPR minimization using the proposed method.

The total computational complexity (CC) of each utilized optimization algorithm was evaluated to show the PAPR minimization performance at a certain CCDF = 10^{-3}. Firstly, the overall complexity expression of the DEHO, DCSA, and DIWO based PTS scheme is achieved as follows:

$$\boldsymbol{CC_{DEHO-PTS}} = 3.\boldsymbol{V}.\boldsymbol{N}.\log_2\boldsymbol{N} + \boldsymbol{C}.\boldsymbol{E}.\boldsymbol{MIN}\ (\boldsymbol{V}-1).\boldsymbol{N}. \tag{26}$$

$$\boldsymbol{CC_{DCSA-PTS}} = 3.\boldsymbol{V}.\boldsymbol{N}.\log_2\boldsymbol{N} + \boldsymbol{S}.\boldsymbol{t}.(\boldsymbol{V}-1).\boldsymbol{N}. \tag{27}$$

$$\boldsymbol{CC_{DIWO-PTS}} = (3.\boldsymbol{V}).\boldsymbol{N}.\log_2\boldsymbol{N} + \boldsymbol{NFE}\ (\boldsymbol{V}-1).\boldsymbol{N}. \tag{28}$$

Secondly, the search complexity of the SLM method (CC_{SLM}), denoted as U, is directly proportional to the amount of IFFT processes achieved during the optimal phase sequence search, and it is represented as follows:

$$\boldsymbol{CC_{SLM}} = (\boldsymbol{U})\ .\ \boldsymbol{N}\ .\log_2\boldsymbol{N}. \tag{29}$$

It's easy to get the computational complexity of modified SLM strategies by taking out the search complexity of SLM given by U from the SLM complexity expression in equation (33) and replacing it with the search complexity of SLM strategies based on intelligence swarm optimization algorithms. The computational complexities of three optimization methods are evaluated accordingly as below:

$$\boldsymbol{CC_{GA-SLM}} = (\boldsymbol{P}\ .\ \boldsymbol{G})\ .\ \boldsymbol{N}\ .\log_2\boldsymbol{N}. \tag{30}$$

$$\boldsymbol{CC_{MBO-SLM}} = [\boldsymbol{W} + (\boldsymbol{W}-\boldsymbol{H}).(\boldsymbol{F}-1)]\ .\boldsymbol{T}.\boldsymbol{C}\ .\ \boldsymbol{N}\ .\log_2\boldsymbol{N}. \tag{31}$$

The computational complexity of any technique, as outlined in equation (30)–(35), is primarily influenced by its search complexity. This research standardizes the computational complexities of the assumed methods by setting their search complexities to a common value of 512. The phase optimization process has enabled intelligent PAPR reduction schemes to achieve a PAPR value of 5.86 dB, surpassing that of the DEHO-SLM method for SN equals 512 at a CCDF of 10^{-3}, $SN = S.t = 2.250 = 500$ for DCSA-SLM, SN = NFE = 480 for DIWO-PTS, SN = 128 for SLM, SN = 112 for GA-SLM, and SN =100 for MBO-SLM. The computational loads required by DCSA-PTS, DIWO-PTS, SLM, GA-SLM and MBO based on SLM to achieve similar PAPR results as the DEHO-PTS are evaluated as (1003008), (964608), (114688), (100352) and (89600), respectively. The computational complexity of the DEHO-PTS method is (1026048) for $SN = 512$, with DCSA-PTS, DIWO-PTS, SLM, GA-SLM and MBO-SLM achieving improvements of 3%, 6%, and 88%, 90% and 91% respectively. The proposed MBO-SLM demonstrates a significant advancement in computational complexity, resulting in a 91% reduction in computational load compared to the DEHO-PTS scheme. This 91% improvement refers to the total CC, defined as the aggregate number of complex additions and multiplications required by the IFFT and phase rotation operations. The complexity is proportional to $O(SN \cdot N \log N)$, where SN is the total search number (candidate sequences evaluated). Because the MBO-SLM algorithm converges to the optimal phase sequence with a significantly lower SN ($SN_{\mathrm{MBO}} \ll SN_{\mathrm{DEHO}}$) for the same target PAPR, the total arithmetic operations are reduced by 91%. The computational complexity of each PAPR reduction method is summarized in table 5.

Table 5. Comparison of search complexity (Search Numbers) for different PAPR reduction techniques.

Methods	Computational complexity	Improvement in percentage (%)
DEHO-PTS	512	0
DCSA-PTS	500	3
DIWO-PTS	480	6
SLM	128	88
GA-SLM	112	90
MBO-SLM	100	91

5.1. Complexity analysis clarification

To accurately quantify the computational advantage of the proposed method, it is essential to translate the Search Number (SN) into the actual computational load and justify the selection of the MBO-SLM control parameters (F, W, H, C, T). Translation of Search Number to Computational Load The Search Number (SN) represents the total number of candidate phase sequences generated and evaluated by the algorithm. In the context of the SLM scheme, each candidate evaluation requires one IFFT operation and one phase rotation sequence. Therefore, the SN translates directly to the total (CC) in terms of complex additions and multiplications as follows:

$$\boldsymbol{CC}_{\text{Total}} \approx \boldsymbol{SN} \times \left(\frac{\boldsymbol{N}}{2}\log_2 \boldsymbol{N} + \boldsymbol{N}\right) \tag{32}$$

where $\frac{N}{2}\log_2 N$ accounts for the N-point IFFT operations and N accounts for the element-wise phase rotations. Consequently, the 91% reduction in complexity reported in this work is derived from the significant reduction in the required SN to achieve a target PAPR level (e.g., 10^{-3} CCDF) compared to the baseline DEHO-SLM and conventional SLM methods. While conventional methods may require thousands of random trials, MBO-SLM converges to the optimal phase vector with a restricted SN (e.g., $SN = 512$), linearly reducing the aggregate arithmetic operations.

5.1.1. Parameter tuning strategy

The MBO-SLM parameters—Flock Size (F), Number of Neighbors (W), Shared Neighbors (H), Tours (T), and Cycles (C)—were tuned to balance the trade-off between exploration (searching new areas of the solution space) and exploitation (refining existing solutions).

- Flock Size (F) & Neighbors (W): F was kept relatively small to minimize the initial computational overhead, while a higher W was selected to ensure thorough local exploitation around each bird (solution).
- Shared Neighbors (H): The sharing parameter H was tuned to facilitate rapid information exchange between the leader and follower birds, preventing the algorithm from getting trapped in local minima and accelerating convergence speed.
- Cycles (C) & Tours (T): These loop parameters were empirically adjusted to determine the 'saturation point' where further iterations provided negligible improvement in PAPR reduction.

6. Conclusion

This research first analyzed and simulated a low cost-effective IM/DD OFDM communication system with 16-QAM modulation using MATLAB and Optisystem software. For PAPR reduction, MBO-SLM was proposed and applied to the IM/DD optical OFDM system. MBO-SLM effectively reduced the PAPR of the original optical OFDM signal, achieving significant improvements over other PAPR reduction methods. The proposed PAPR reduction method achieves a PAPR reduction gain of 5.55 dB compared to the original OFDM signal at a CCDF of 10^{-3} while the search number is 512. The proposed PAPR reduction method is tested to show its effect on the PAPR reduction performance for different high QAM modulation orders. For instance, at a CCDF of 10^{-3}, the difference in PAPR among different M-QAM orders is 0.05 dB. The parameters of the MBO-SLM algorithm, such as number of initial solutions (F), number of neighboring solutions to be assumed (W), number of neighboring solutions to be shared with the following solution (H), number of tours (T), and number of cycles (C) affect the PAPR performance of our proposed OFDM system. Simulation results demonstrated that the best PAPR minimization performances were obtained with the lowest bird numbers

Table 6. Abbreviations.

ACO-OFDM	Asymmetrically clipped Optical-OFDM
ADO-OFDM	Asymmetrically clipped DC-biased optical-OFDM
BER	Bit Error Ratio
C (for DEHO-PTS)	Number of clans
C (for MBO-SLM)	Max. cycle number
CO-OFDM	Coherent Detection OFDM
CCDF	Complementary Cumulative Distribution Function
DFT	Discrete Fourier Transform
DEHO	Discrete Elephant Herding Optimization
DCSA	Discrete Crow Search Algorithm
DIWO	Discrete Invasive Weeding Optimization
E (for DEHO-PTS)	Number of elephants
F (for MBO-SLM)	Number of initial solutions
FFT	Fast Fourier Transform
FT	Fourier Transform
F (for MBO-SLM)	Total amount of birds in the swarm.
G (for GA-SLM)	Number of generations
GA-SLM	Genetic Algorithm - SLM
HS	Hermitian symmetry
H (for MBO-SLM)	The number of adjacent solutions shared by members of the population.
IM/DD	Intensity Modulation/Direct Detection
IFFT	Inverse Fast Fourier Transform
LM-DDO-OFDM	Linearly Mapped DDO-OFDM
MBO	Migrating Birds Optimization
MIN (for DEHO-PTS)	Maximum number of iterations
NFE (for DIWO-PTS)	Number of fitness evaluations
NLM-DDO-OFDM	Nonlinearly Mapped DDO-OFDM
OTR	Optical to RF
RTO	RF to optical
P (for GA-SLM)	Population size
PI	Peak Insertion
OFDM	Orthogonal Frequency Division Multiplexing
PAPR	Peak-to-Average Power Ratio
PTS	Partial Transmit Sequence
QAM	Quadrature Amplitude Modulation
T (for MBO-SLM)	Max. tour number
t (for DCSA-PTS)	Maximum number of iterations
S (for DCSA-PTS)	Population size
SCF	Simplified clipping and filtering
SLM	Selective Mapping
TI	Tone Reservation
VLC	Visible Light Communication
U (for SLM)	Number of phase vectors
W (for MBO-SLM)	The amount of neighbor solutions generated for every element of the population.

combinations. The proposed PAPR reduction method enhances spectral efficiency, signal integrity, and reduces data errors, thereby improving overall performance and reliability in optical communication systems. When the BER is set at 10^{-4}, the MBO-SLM technique requires approximately 1.5 dB less OSNR compared to the GA-SLM technique. It also demands about 2.86 dB less OSNR than the conventional SLM technique, around 4.3 dB less than the DIWO-PTS technique, about 5.7 dB less than the DCSA-PTS technique, roughly 8.1 dB less than the DEHO-PTS technique, and approximately 9 dB less than the original OFDM signal. Overall, the MBO-SLM technique demonstrates superior BER performance relative to other methods. Finally, the computational complexity of the MBO-SLM method shows a 91% improvement over the DEHO-PTS method when the search number is set to 512. While this study demonstrates the theoretical efficiency of MBO-SLM via simulation, real-time hardware implementation faces challenges such as processing latency and synchronization. As highlighted in [43], practical implementation on platforms like Software-Defined Radio (SDR) requires careful consideration of these hardware-specific constraints. Future research will focus on enhancing the MBO-SLM framework by hybridizing the MBO algorithm with mutation-based operators, such as Cauchy and Gaussian mutations. By integrating these operators, we aim to balance the algorithm's exploration and exploitation phases more effectively, potentially achieving superior PAPR reduction with reduced

computational iterations. This strategy is supported by recent advancements in hybrid metaheuristics; for instance [44], demonstrated that incorporating Cauchy mutation into PSO significantly prevents premature convergence in hybrid clipping-PTS schemes. Ultimately, exploring these hybridizations will align the proposed method with state-of-the-art signal processing strategies, ensuring robust global search capabilities in increasingly complex communication environments.

The definitions of the abbreviations can be found in table 6.

Statements and declarations

Declaration of competing interest

The authors state that they have no known conflicting financial interests or relationships that might have influenced the research presented in this paper.

Funding

This publication was supported by the Scientific Research Projects Coordination Unit of Istanbul Yeni Yuzyil University.

Data availability statement

The data that support the findings of this study are available upon reasonable request from the authors.

Author contributions

Mahmoud Alhalabi 0000-0002-6532-9881
Methodology (equal), Software (equal), Writing – original draft (equal)

Necmi Taşpınar
Supervision (equal)

Mohammed Wadi
Supervision (equal), Writing – review & editing (equal)

References

[1] Kong X, Guan H, Jiang L, Wang Y and Zhang C 2024 Icing detection on ADSS transmission optical fiber cable based on improved YOLOv8 network *Signal Image Video Process* **18** 5323–32
[2] Sharif A 2019 PAPR reduction of optical OFDM signals in visible light communications *ICT Express* **5** 202–5
[3] Mhatre K 2015 Efficient selective mapping PAPR reduction technique *Procedia Comput. Sci.* **45** 620–7
[4] Ahmed I, Karvonen H, Kumpuniemi T and Katz M 2020 Wireless communications for the hospital of the future: requirements, challenges and solutions *Int. J. Wirel. Inf. Networks* **27** 4–17
[5] Chaaban A, Rezki Z and Alouini M 2022 On the capacity of intensity-modulation direct-detection gaussian optical wireless communication channels *IEEE Commun. Surv. Tutorials* **24** 455–91
[6] Hameed S, Sabri A and Abdulsatar S 2021 A novel PAPR reduction method for ADO-OFDM VLC systems *Opt. Quantum Electron.* **53** 553
[7] Chen L, Krongold B and Evans J 2012 Performance analysis for optical OFDM transmission in short-range IM/DD systems *J. Lightwave Technol.* **30** 974–83
[8] Singhal S and Sharma D 2024 A review and comparative analysis of PAPR reduction techniques of OFDM system *Wirel. Pers. Commun.* **135** 777–803
[9] Mondal S 2021 Approach to reduce PAPR in orthogonal frequency division multiplexing technique *Turk J. Comput. Math. Educ.* **12** 4480–4
[10] Noursabbaghi B, Baghersalimi G, Pouralizadeh A and Mohammadian O 2023 PAPR reduction in OFDM UOWC system employing repetitive clipping and filtering (RCF) method *J. Electr. Comput. Eng. Innov.* **11** 301–10
[11] Rana M, Tithy T, Rahman N and Hasan M 2022 PAPR reduction techniques and their bit error rate measurement at OFDM in LTE system *Int. J. AdHoc Netw. Syst.* **12** 1–12
[12] Faraj B and Siddiq A 2022 Peak to average power ratio reduction for OFDM with IM system *Proc. 2022 4th Int. Conf. Adv. Sci. Eng.* **95** 100
[13] Abdulhussein A and Hikmat N 2021 Comparative study of peak to average power ratio in OFDM and FBMC systems *Proc. 2021 7th Int. Conf. Space Sci. Commun.* **140** 145

[14] Krikunov S, Bychkov R, Blagodarnyi A and Ivanov A 2023 Clustering and fitting to reduce PAPR in multi-user OFDM systems *Proc. 25th Int. Conf. Digit. Signal Process. Appl.* 1–6
[15] Prasad S and Arun S 2023 Hanowa matrix based SLM technique for PAPR reduction in OFDM systems *Proc. 2023 Int. Conf. Adv. Technol.* 1–5
[16] Priyanka P, Shaik R, Vijaya K, Sasi P, Ruthvik P and Raja A 2023 Improved MFO algorithm-based PTS scheme in OFDM systems for PAPR reduction *Proc. 4th Int. Conf. Signal Process. Commun.* 153–7
[17] Ishmiev I and Loginov S 2023 M-sequence based partial transmit sequence PAPR reduction technique *Proc. Syst. Signals Gener. Process. Field on Board Commun.* 1–5
[18] Tu Y and Chang C 2023 A novel low complexity two-stage tone reservation scheme for PAPR reduction in OFDM systems *Sensors* **23** 950
[19] Yuan Y, Wei S, Luo X, Xu Z and Guan X 2022 Adaptive PTS scheme based on fuzzy neural network for PAPR reduction in OFDM system *Digit. Signal Process.* **126** 103492
[20] Padarti V, Dasari C, Dokala P, Chowtapalli V and Avula L 2022 An efficient clipping method for PAPR reduction in OFDM systems *Proc. Int. Conf. Invent. Comput. Technol.* 624–9
[21] Ramadevi D and Rao P T 2022 Maximal-Minimum hybrid approach with decomposed SLM technique for 5G UFMC system PAPR reduction *Optik* **270** 169955
[22] Niwareeba R, Cox M and Cheng L 2022 Low complexity hybrid SLM for PAPR mitigation for ACO *OFDM ICT Express* **8** 72–6
[23] Karthika J, Thenmozhi G and Rajkumar M 2021 PAPR reduction of MIMO-OFDM system with reduced computational complexity SLM scheme *Mater. Today Proc.* **37** 2563–6
[24] Mayakannan A, Arvind C, Dhinakar P, Sasikala G, Sathyasri B, Srihari K and Shanmuganathan V 2022 Neural network-based regression assisted PAPR reduction method for OFDM *Systems Sādhanā* **47** 242
[25] Yu J, Liu J, Ma Y and Liu Z 2021 PAPR reduction in OFDM system using a new quantum genetic algorithm *Proc. 2021 5th Int. Conf. Electron. Inf. Technol. Comput. Eng.* 1056, 1060 10.1145/3457682.3457887
[26] Zou F, Liu Z, Xin H and Wang G 2021 A novel PAPR reduction scheme for OFDM systems based on neural networks *Wirel. Commun. Mob. Comput.* **2021** 5574807
[27] Xing Z, Liu K, Rajasekaran A, Yanikomeroglu H and Liu Y 2021 A hybrid companding and clipping scheme for PAPR reduction in OFDM systems *IEEE Access* **9** 61565–76
[28] Bäuml R, Fischer R and Huber J 1996 Reducing the peak-to-average power ratio of multicarrier modulation by selected mapping *Electron. Lett.* **32** 2056–7
[29] Wang C and Ouyang Y 2005 Low-complexity selected mapping schemes for peak to-average power ratio reduction in OFDM systems *IEEE Trans. Signal Process.* **53** 4652–60
[30] Alhalabi M, Taşpınar N and Wadi M 2025 PAPR reduction using discrete forest optimization algorithm based on SLM technique in ıntensity modulated direct detection optical OFDM communication systems *Int. J. Commun. Syst.* **38** e70126
[31] Alhalabi M, Taşpınar N and El-Nahal F I 2023 Bidirectional intensity modulated/direct detection optical OFDM WDM-PON system *Optoelectron. Lett.* **19** 83–7
[32] Taspınar N and Alhalabi M 2021 Performance investigation of long-haul high data rate optical OFDM IM/DD system with different QAM modulations *J. Electr. Eng.* **72** 192–7
[33] Alhalabi M, Taşpınar N and Wadi M 2026 Performance analysis of a low-cost directly modulated OFDM-based optical wireless communication systems *Wirel. Pers. Commun.* **140** 1–18
[34] Alhalabi M and Taşpınar N 2022 Performance ınvestigation of bidirectional hybrid long-haul optical IM/DD OFDM WDM-PON using OOK-RSOA remodulation *Müh. Bilim. Araştırma. Derg.* **4** 54–61
[35] Alhalabi M, El-Nahal F I and Taşpınar N 2019 Comparison of different modulation techniques for optical OFDM ıntensity modulation and direct detection IM/DD system *2019 IEEE 7th Palestinian Int. Conf. on Electrical and Computer Engineering (PICECE)* (IEEE) 1–4
[36] Taşpınar N and Şimşir Ş 2020 An efficient SLM technique based on migrating birds optimization algorithm with cyclic bit flipping mechanism for PAPR reduction in UFMC waveform *Phys. Commun.* **43** 101225
[37] Moharam M H and Wafik A W 2024 Deep learning ıntegration in PAPR reduction in 5G filter bank multicarrier systems *Int. J. Electr. Electron. Eng.* **20** 115–25
[38] Kabli A and Faqihi M 2018 Optical OFDM (O-OFDM) for intensity modulated/direct detection optical systems *Proc. 2018 IEEE Int. Conf. Commun. Networks Satell.* 34–8
[39] Abdulkafi A, Alias M, Hussein Y and Omar N 2017 PAPR reduction of DC biased optical OFDM using combined clipping and PTS techniques *Proc. 2017 IEEE 13th Malaysia Int. Conf. Commun.* 1–6
[40] Freag H, Hassan E, El-Dolil S and Dessouky M 2018 New hybrid PAPR reduction techniques for OFDM based visible light communication systems *J. Opt. Commun.* **39** 427–35
[41] Duman E, Uysal M and Alkaya A 2012 Migrating birds optimization: a new metaheuristic approach and its performance on quadratic assignment problem *Inf. Sci.* **217** 65–77
[42] Taşpınar N and Alhalabi M 2024 Peak-to-average power ratio (PAPR) reduction using discrete ınvasive weed optimization (DIWO) in coherent detection optical OFDM (CO-OFDM) communication systems *Wirel. Pers. Commun.* **139** 715–32
[43] Gouda M E, Mansour A and El-Kordy M 2017 USRP ımplementation of PTS technique for PAPR reduction in OFDM using LABVIEW *Adv. Wirel. Commun. Netw.* **2** 15–24
[44] Moharam M H, Gouda M and El Hennawy H M 2019 Hybrid clipping-PTS using enhanced PSO with Cauchy mutation to reduce PAPR of FBMC 5G systems *Int. J. Syst. Control Commun.* **10** 147–75